

INDIRECT MATRIX CONVERTER BASED SINGLE STAGE HIGH
FREQUENCY LINK PWM AC/AC CONVERTER WITH SOURCE
BASED COMMUTATION OF LEAKAGE ENERGY

A THESIS
SUBMITTED TO THE FACULTY OF
UNIVERSITY OF MINNESOTA
BY

Arushi Shahani

IN PARTIAL FULFILLMENT OF THE REQUIREMENTS
FOR THE DEGREE OF
MASTER OF SCIENCE

Professor Ned Mohan

May 2013

© Arushi Shahani 2013
ALL RIGHTS RESERVED

Acknowledgements

I am grateful to Professor Ned Mohan, my research and academic advisor for his constant support and guidance. I thank him for his continuous encouragement and consider myself lucky to have had the opportunity to work in his research group. He is very passionate about education and research in power electronics and he is an inspiration for me.

I am thankful to Professor William Robbins and Professor Anand Tripathi for being a part of my oral examination committee and for their valuable input towards my work.

I would like to thank Dr. Kaushik Basu, my colleague in the power electronics lab for his help and guidance in my research project. I would also like to thank all my colleagues for their help.

On a personal note I would like to thank my parents, family and friends for their continuous encouragement and support. I would specially like to thank Mr. G. Chhibbar for his constant support and for always motivating me to do better in life.

Dedication

To my parents Professor D.T. Shahani and Professor Vibha and my late grandmother Smt Prem Manjusha for their unconditional love and support and specially for teaching me the value of education.

Abstract

High frequency AC link three phase AC to three phase adjustable speed and magnitude PWM AC converters with single stage power conversion and bidirectional power flow are important in modern power distribution system and as a compact solution to grid connected adjustable speed drives (traction, wind). Due to the use of high frequency these types of converters achieve high power density. Open loop power factor correction, higher efficiency and reliability are important features of these types of converters. One major problem in this type of converter is the commutation of leakage energy which results in power loss, reduction in switching frequency, distortion and loss of output voltage. The topology based on the indirect modulation of matrix converters uses minimum amount of copper and has relatively less number of semiconductor switches. This thesis presents a lossless source based commutation strategy along with a modulation technique that minimizes the frequency of leakage inductance commutation. It also results in the soft switching of the output converter (Zero current switching: ZCS). The topology along with the proposed control has been analyzed, simulated and verified through experimental results. Simulation and experimental results confirm the operation.

Contents

Acknowledgements	i
Dedication	ii
Abstract	iii
List of Tables	vi
List of Figures	vii
1. Introduction	1
2. Modulation	5
2.1 Matrix converter	5
2.2 Current source inverter	8
2.3 Voltage source inverter	12
2.4 Indirect modulation of matrix converter	16
2.5 Modulation scheme of the proposed topology	18
3. Commutation	21
3.1 Commutation when output converter switches from one active vector to next	22
3.2 Commutation due to the transition of the flux balance signal	24
4. Simulation Results	25
4.1 Parameters used in simulation	25
4.2 Results of simulation	25

5. Experimental Results	29
5.1 Experimental setup	29
5.2 Experimental results	30
5.3 Comparison of analytic and experimental results	33
6. Conclusion	34
References	35

List of Tables

1. Combined switching states of CSI and VSI	17
2. Parameters for simulation	25
3. Parameters in experimental setup	30

List of Figures

1. Wind power application	2
2. A four quadrant switch	5
3. Four step commutation	5
4. Matrix converter	6
5. Current source inverter	8
6. CSI with switching state [a b]	10
7. Space vector representation of CSI	11
8. IGBT with anti-parallel diode	12
9. Voltage source inverter	12
10. Space vector representation of VSI	13
11. VSI with switching state [1 1 0]	15
12. Indirect modulation of matrix converter	17
13. Circuit diagram of power electronic converter system	18
14. Generation of switching signals	19
15. Application of voltage and current vectors over T_s	20
16. Commutation when output converter switches from one active vector to next	22
17. Commutation due to the transition of the flux balance signal	23
18. Simulation result: output line to neutral voltage and output line current	26
19. Simulation result: (a) input line to neutral voltage with filtered input line current (20 A/div) (b) actual input line current	26
20. Simulation result: commutation of leakage inductance current	27
21. Simulation result: magnetizing current	28
22. Input line voltage CH1 (20V/div), and input current CH4 (5A/div)	31
23. Output line to neutral voltage CH3 (50 V/div), line currents CH1, CH2 and CH4 (5A/div) and time (50 ms/div)	31

24. Input line to neutral voltage CH3 (50 V/div), line currents CH1, CH2 and CH4 (5A/div) and time (50 ms/div)	32
25. Control voltage (S Signal) CH3 (10V/div), primary voltage CH1 (100V/div), leakage inductance current CH4 (5A/div) and time (50 μ S/div)	32
26. Expanded view of the waveform in figure 25	33

Chapter 1

Introduction

Transformers are typically used to connect systems at different voltage levels and to provide galvanic isolation often necessary for safety requirements. In high power systems line frequency transformer tends to be the largest and the most expensive component. Replacement of the low frequency transformer with its high/medium frequency counterpart along with power electronic converters leads to dramatic increase in power density. Steady reduction in the cost of semiconductor switches and availability of advanced magnetic materials with high flux density and low loss density leads to the possibility of feasible design with comparable efficiency and economic viability. These high frequency link AC/AC power converters are known as power electronic transformers (PET) / solid state transformers (SST) [1]. PETs can be employed in modern power distribution systems due to advanced features like reactive power support, voltage and frequency control etc. Due to additional features like on demand reactive power support, voltage and frequency regulation etc., PETs have been identified as an enabling technology for the modernization of the electric power distribution system [2] [3]. Another major area of application is high power density electric motor drives for example in a) electric traction [4] [5] [6] b) wind power [7] [8] and c) medium voltage ASDs [9].

In vertical wind turbines a PET can be placed at the top of the tower, and can replace the low frequency transformer located at the bottom of the tower and eliminate the significant copper loss incurred in carrying the generated power from the top to the bottom of the tower at a low voltage and high current while still maintaining a compact Nacelle structure, Figure 1.

Part of this thesis has been taken from [37]

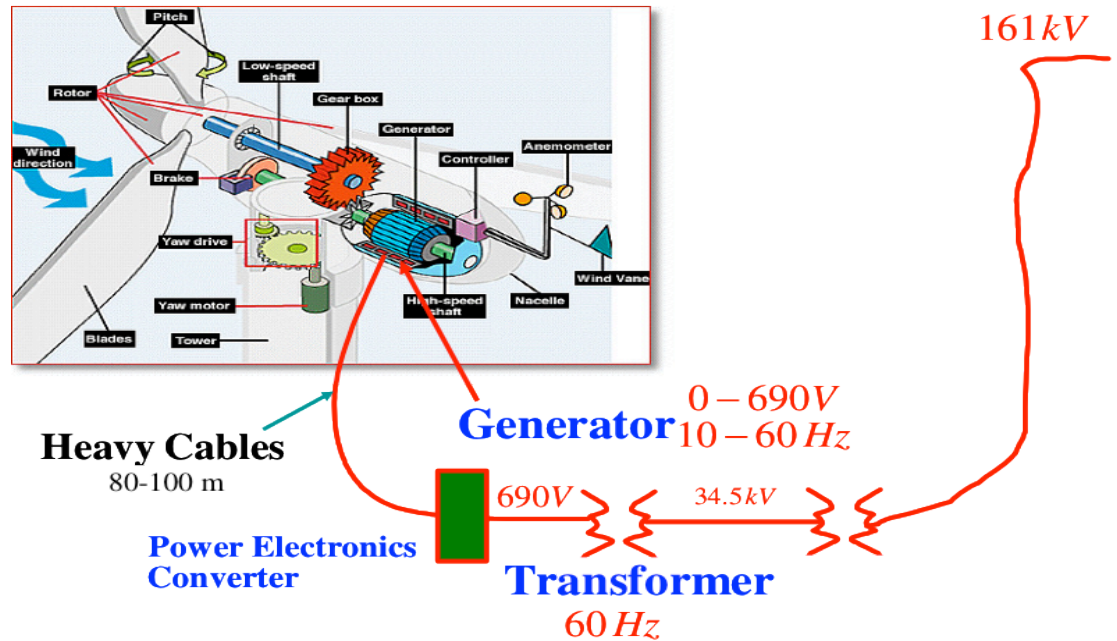


Figure 1. Wind power application

[10] [11] provides detailed classification of different types of PETs. Two stage PETs are of two kinds - high voltage DC link (HVDC) [12] [13] and low voltage DC link (LVDC) [4] [5] [6]. A three stage PET usually has a high frequency link DC/DC converter [14] [15] [16] [17]. To match with the grid voltage and rated power these topologies either use series parallel connection of modular units or use multi-level structures. Due to multi stage configuration these topologies usually experience reduction in efficiency, reliability and power density.

Single stage Single phase AC/AC PETs (based on full- bridge [18] [19] [20] [21] or fly-back converters [22]) are fixed frequency and do not provide power factor correction [10]. A three phase version of flyback converter can be found in [23]. Single [24] and three-phase [25] resonant (Dual Active Bridge-DAB) converter based PETs have the additional limitations of higher conduction loss, THD and sensitivity of the active power flow on the leakage inductance.

Three-phase single stage PETs are primarily based on matrix converter [26] and

provide an all silicon solution with grid power factor control and adjustable magnitude and frequency PWM voltage generation. These types of PETs are classified into three types [27]. In the first type of PET the input converter simply chops the input AC grid voltage to 50 % duty-cycle high frequency AC and passes it through a bank of three high frequency transformers (HFTs). The load side converter operates as matrix converter to generate three-phase PWM AC at the load end [28]. The push-pull structure in the input side converter results in a reduced number of switches. Reduced switch count and soft switching of the grid side converter (high voltage blocking slow devices) are the major advantages [29]. In the other type, modulation is done in the primary side and the secondary or load side converter is simplified [30]. This topology has the advantages of source based commutation of leakage energy, common-mode voltage elimination and minimization of the effect due to leakage energy commutation. One of the major disadvantages of this topology is the presence of large number of switches. The third type of PET is based on the indirect modulation [31] of matrix converters and is the focus of this thesis.

In this type of PET [32] [33], the virtual DC link of an indirect matrix converter is chopped with a 50 % duty-cycle by the grid side converter and passed through a single phase HFT. The load side converter first rectifies the high frequency AC to get back the virtual DC link and then inverts it to generate adjustable speed and magnitude PWM AC at the load end. This type of converter uses least amount of copper and has fairly small number of switch count when compared with other two types.

The windings of the high frequency transformer have leakage inductance. Any transition of the secondary side needs commutation of leakage energy resulting in output voltage loss, common mode voltage switching and reduction in switching frequency. In this work a novel PWM technique has been developed to minimize the frequency of leakage commutation in this type of PET.

Commutation of leakage energy by additional snubber circuits results in loss of the leakage energy and reduction in reliability and power density. Source based commutation of leakage energy has been analyzed in high frequency link DC/AC [34]

and single-phase AC/AC HF link converters [35]. Source based commutation is not possible in the first type of PET due to push pull structure [36].

In this thesis a source based commutation of leakage energy has been developed. It leads to the elimination of any additional snubber circuits, soft switching of the load side converter and partial recovery of the leakage energy.

A part of this work has been published in [37].

Chapter 2

Modulation

2.1 Matrix converter

A matrix converter converts a balanced three phase AC voltage to balanced three phase pulse width modulated (PWM) AC voltage with adjustable magnitude and frequency. In a matrix converter one leg consists of three switches and each switch is four quadrant as it blocks voltage in both directions and allows bidirectional current flow. The switch is implemented as a common emitter connection of two IGBTs as shown in Figure 2. The switching of one leg is done using four-step commutation.

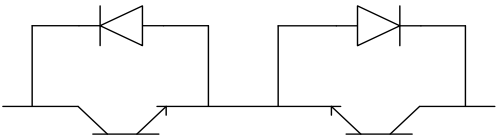


Figure 2. A four quadrant switch

The procedure of 4-step commutation is as follows (here the case when leg current is positive is considered, $i > 0$). In Figure 3 Q1 and Q2 are the conducting pair of IGBTs and Q3 and Q4 are the non-conducting pair of IGBTs.

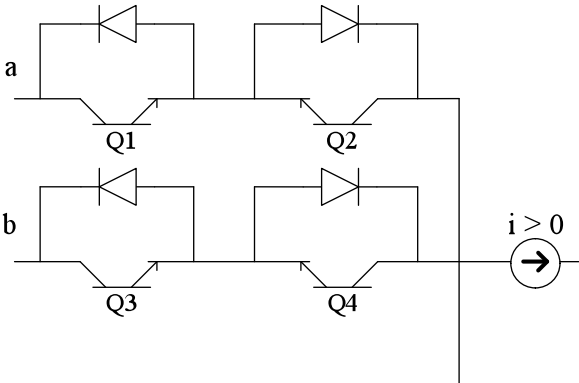


Figure 3. Four step commutation

Step 1 : Turn off Q2.

Step 2 : Turn on Q3. If $V_{ab} > 0$ then no switching takes place otherwise ($V_{ab} < 0$) natural commutation will occur.

Step 3 : Turn off Q1.

Step 4 : Turn on Q4.

Matrix converter as shown in Figure 4 has 27 different allowed switching states out of which there are 3 zero states, 6 synchronously rotating states and 18 other states. These 18 states are used in indirect modulation of matrix converter.

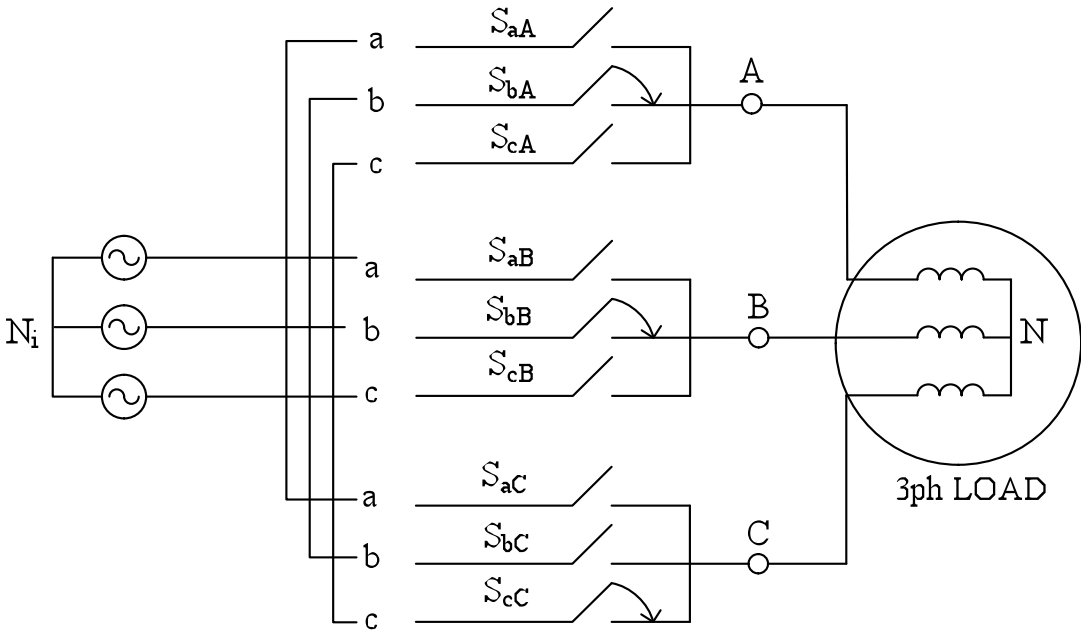


Figure 4. Matrix converter

Each leg in a matrix converter is switched independently. In one leg only one switch can be on at a point of time to avoid short circuiting the input source voltage. Also in one leg of matrix converter at least one switch should be on all the time to ensure continuity of the leg current. Say in Figure 4, S_{bA} , S_{bB} and S_{cC} are on, that means the switching state is [b b c].

The 27 possible switching states of a matrix converter are:

1. Zero states

[a a a]

[b b b]

[c c c]

2. Synchronously rotating states

[a b c]

[a c b]

[b a c]

[b c a]

[c a b]

[c b a]

3. 18 switching states used in indirect modulation of matrix converter

[a a b]

[a a c]

[b a a]

[b c c]

[c a a]

[c b b]

[a b a]

[a c a]

[b a b]

[b c b]

[c a c]

[c b c]

[b b a]

[c c a]

[b b c]

[c c b]

[a c c]

[a b b]

As the proposed converter's control is based on indirect modulation of matrix converter, first the indirect modulation of matrix converter is described in detail. In order to understand indirect modulation of matrix converter it is important to understand modulation of Current Source Inverter (CSI) and Voltage Source Inverter (VSI).

2.2 Current source inverter

The CSI converts DC current to three phase balanced PWM AC currents. It consists of two legs as shown in Figure 5 where the top leg has switches S_{a1} , S_{b1} and S_{c1} and the bottom leg has switches S_{a2} , S_{b2} and S_{c2} . At least one switch should be on in each leg. Also not more than one switch should be on in each leg.

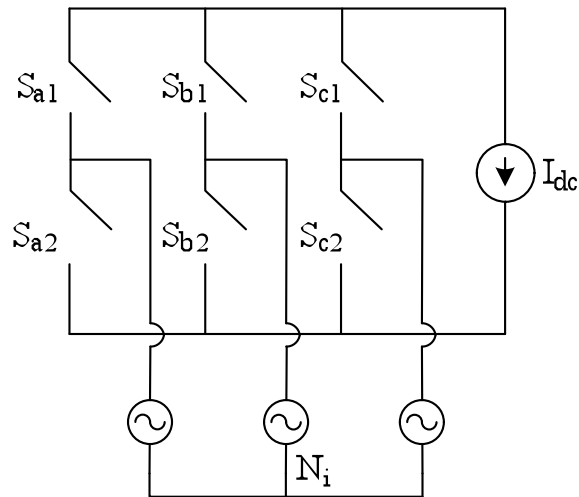


Figure 5. Current source inverter

V_{IN} is the peak of the input voltage, I_{IN} is the peak of the average input current and ω_i is the input frequency. (1) gives the three phase balanced line to neutral voltages. (2) gives the fundamental components of the input line currents. Input line current space vector is defined in (3) and (4) gives the input line current space vector (\bar{i}_{IN}) averaged over a sampling cycle T_s .

$$\begin{aligned} v_{aNi} &= V_{IN} \cos \omega_i t \\ v_{bNi} &= V_{IN} \cos \left(\omega_i t - \frac{2\pi}{3} \right) \end{aligned} \quad (1)$$

$$\begin{aligned} v_{cNi} &= V_{IN} \cos \left(\omega_i t + \frac{2\pi}{3} \right) \\ \bar{i}_a &= I_{IN} \cos \omega_i t \\ \bar{i}_b &= I_{IN} \cos \left(\omega_i t - \frac{2\pi}{3} \right) \end{aligned} \quad (2)$$

$$\begin{aligned} \bar{i}_c &= I_{IN} \cos \left(\omega_i t + \frac{2\pi}{3} \right) \\ i_{IN} &= i_a + i_b e^{j\frac{2\pi}{3}} + i_c e^{-j\frac{2\pi}{3}} \end{aligned} \quad (3)$$

$$\bar{i}_{IN} = \frac{3}{2} I_{IN} e^{j\omega_i t} \quad (4)$$

A CSI consists of 9 switching states, 6 active states and 3 zero states.

1. Zero states

[a a]

[b b]

[c c]

2. Six active states

[a b]

[a c]

[b a]

[b c]

[c a]

[c b]

Say in the top leg of CSI S_{a1} is on and in the bottom leg of CSI S_{b2} is on, this represents the switching state [a b] as shown in the following Figure 6.

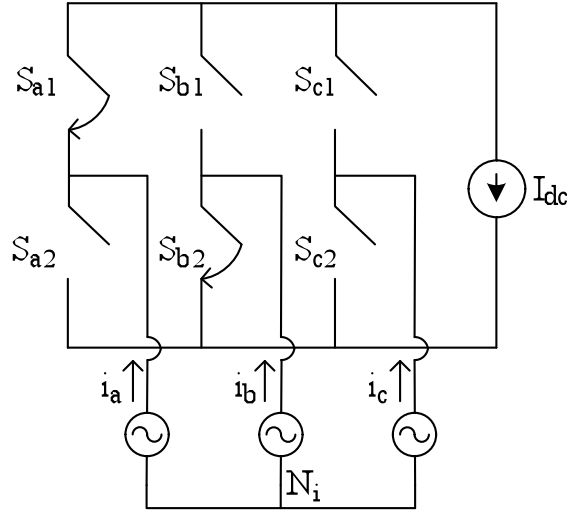


Figure 6. CSI with switching state [a b]

Say we take example of the switching state $I_{[a,b]}$

$$i_a = I_{dc} \quad i_b = -I_{dc} \quad i_c = 0$$

$$\begin{aligned} I_{[a,b]} &= I_{dc} - I_{dc} e^{j\frac{2\pi}{3}} \\ &= I_{dc} - I_{dc} \left[\cos\frac{2\pi}{3} + j \sin\frac{2\pi}{3} \right] \\ &= \frac{3}{2} I_{dc} - j \frac{\sqrt{3}}{2} I_{dc} \\ &= \sqrt{3} I_{dc} \left[\frac{\sqrt{3}}{2} - \frac{1}{2} j \right] \\ &= \sqrt{3} I_{dc} e^{-j\frac{\pi}{6}} \end{aligned}$$

Similarly for all the different switching states the current space vector can be obtained and all of them have a magnitude of $\sqrt{3} I_{dc}$. The current space vectors are depicted in Figure 7 where I_1 is the space vector of switching state [a b], I_2 for [a c], I_3 for [b c], I_4 for [b a], I_5 for [c a] and I_6 for [c b].

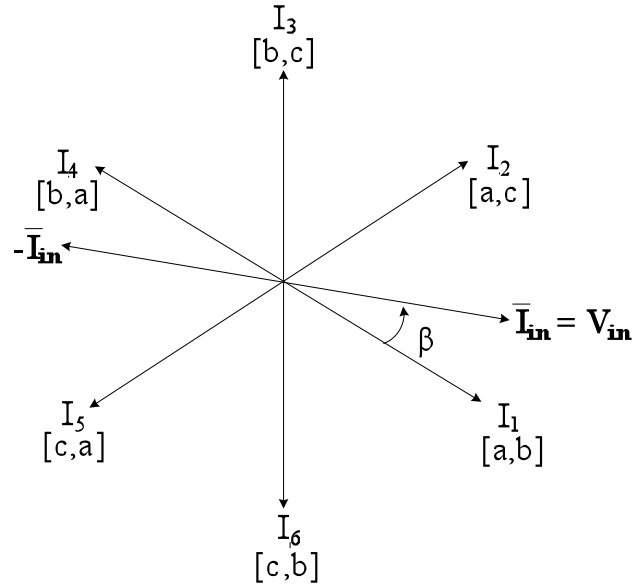


Figure 7. Space vector representation of CSI

Switching of the input converter is done such that the average input line current space vector is in phase with the input voltage space vector. This results in unity power factor. This means that the angle between the input average current space vector and that of the input voltage vector or the input power factor angle is set to zero so we can get unity power factor. The angle of the average reference current vector is obtained by sensing the input voltage space vector. The modulation index is given in (5). It is set to the maximum value of one. Depending on which sector is the average input current vector located we can find out which two vectors will be applied. If the average input current space vector lies in the first sector i.e. between I_1 and I_2 then I_1 will be applied for dI_1T_s period of time and I_2 for dI_2T_s period of time. Here dI_1 and dI_2 are duty ratios as shown in (6).

$$m_I = \frac{I_{in}}{I_{dc}} \quad (5)$$

Averaged over a cycle

$$\frac{3}{2} I_i e^{j\beta} = dI_1 \sqrt{3} I_{dc} + dI_2 \sqrt{3} I_{dc} e^{j\frac{\pi}{3}}$$

$$dI_1 = \left(\frac{I_i}{I_{dc}} \right) \sin(60 - \beta) \tag{6}$$

$$dI_2 = \left(\frac{I_i}{I_{dc}} \right) \sin \beta$$

2.3 Voltage source inverter

In this section modulation of a VSI with space vector modulation is presented. VSI consists of three legs. Each leg consists of series connection of two IGBTs with anti parallel diode. Each switch in a VSI allows bidirectional current flow and blocks voltage in only one direction. The switch is shown in Figure 8 and VSI is shown in Figure 9. From a DC voltage source we generate a three phase balanced adjustable magnitude and frequency PWM AC voltage.

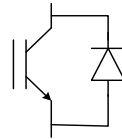


Figure 8. IGBT with anti parallel diode

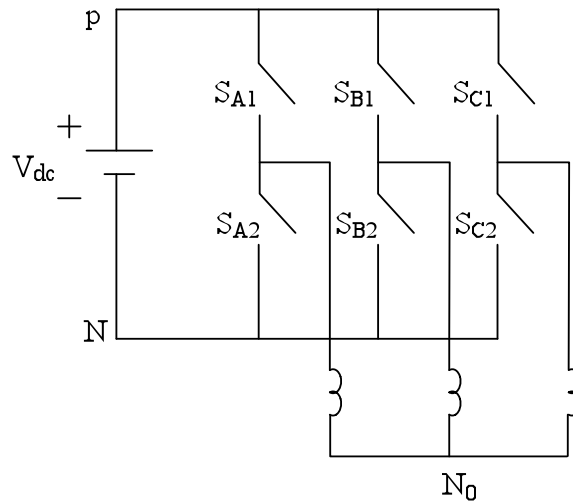


Figure 9. Voltage source inverter

(7) defines the output voltage space vector. (8) presents average three phase balanced line to neutral voltages (V_o is the peak and ω_o is the angular frequency) to be synthesized by the VSI. (9) shows the constant magnitude synchronously rotating average output voltage vector V_{ref} that is generated by switching the VSI.

$$V_o = v_{AN_o} + v_{BN_o} e^{j\frac{2\pi}{3}} + v_{CN_o} e^{-j\frac{2\pi}{3}} \quad (7)$$

$$\begin{aligned} \bar{v}_{AN} &= V_o \cos(\omega_o t + \phi_o) \\ \bar{v}_{BN} &= V_o \cos\left(\omega_o t - \frac{2\pi}{3} + \phi_o\right) \\ \bar{v}_{CN} &= V_o \cos\left(\omega_o t + \frac{2\pi}{3} + \phi_o\right) \end{aligned} \quad (8)$$

$$\begin{aligned} V_{ref} &= \bar{v}_{AN_o} + \bar{v}_{BN_o} e^{j\frac{2\pi}{3}} + \bar{v}_{CN_o} e^{-j\frac{2\pi}{3}} \\ &= \frac{3}{2} V_o e^{j(\omega_o t + \phi_o)} \end{aligned} \quad (9)$$

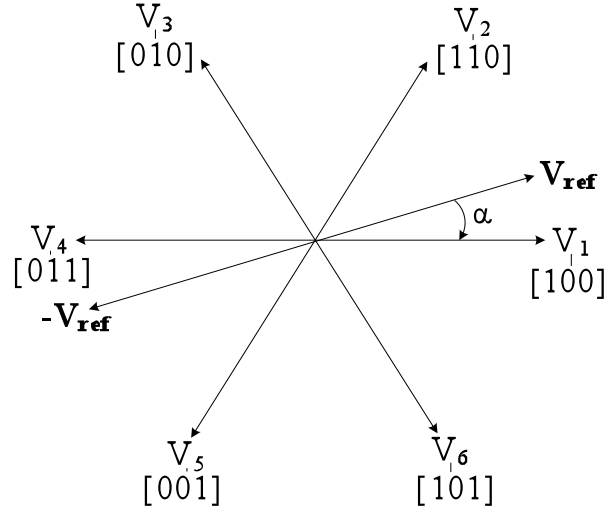


Figure 10. Space vector representation of VSI

In order to avoid short circuiting of the input DC source and the interruption of the inductive leg or the line current, the two switches in each leg of the VSI are switched in a complementary fashion. This results in 8 switching states, 6 active states and 2 zero states as shown in Figure 10.

The switching states of a VSI are:

Zero states

[0 0 0]

[1 1 1]

Active states

[1 0 0]

[1 1 0]

[0 1 0]

[0 1 1]

[0 0 1]

[1 0 1]

A switching state [1 1 0] implies S_{A1} , S_{B1} and S_{C2} are on as shown in Figure 11. As the neutral of the three-phase load is the floating, sum of the three line currents must be zero ($i_A + i_B + i_C = 0$). As the load is balanced it is possible to express the line neutral voltages in terms of the pole voltages as shown in (10). Note when state [1 1 0] is applied $v_{aN} = V_{dc}$, $v_{bN} = V_{dc}$ and $v_{cN} = 0$. By using (10) and (7) it is possible to show that $\vec{V}_o = V_{dc} e^{j\frac{\pi}{3}}$. This is the vector V_2 corresponding to the active state [1 1 0]. Similarly it is possible to compute voltage vectors corresponding to all other five active switching states. These vectors are shown in figure (9). These six active vectors divide the space vector plane in six symmetrical sectors.

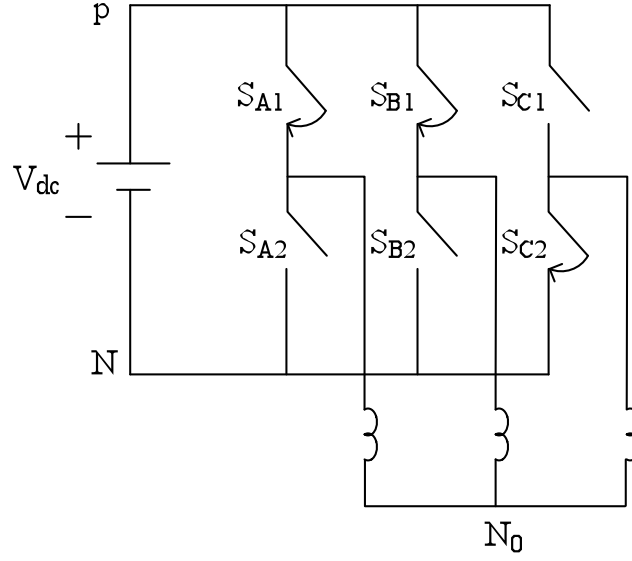


Figure 11. VSI with switching state [1 1 0]

$$\begin{aligned}
 v_{aN_0} &= \frac{1}{3}(2v_{aN} - v_{bN} - v_{cN}) \\
 v_{bN_0} &= \frac{1}{3}(2v_{bN} - v_{cN} - v_{aN}) \\
 v_{cN_0} &= \frac{1}{3}(2v_{cN} - v_{aN} - v_{bN})
 \end{aligned} \tag{10}$$

At a particular sampling cycle depending on which sector is the output voltage vector V_{ref} is located we can find out which two vectors have to be applied. The two active vectors forming that particular sector are applied on an average to synthesize V_{ref} . For example if the average output voltage vector lies in the first sector i.e. between V_1 and V_2 then V_1 will be applied for dV_1T_s period of time and V_2 for dV_2T_s period of time. α is the position of the output voltage vector V_{ref} with respect to the first vector V_1 . m_v is the modulation index given in (11) and dV_1 and dV_2 are the duty ratios over T_s given in (12).

$$m_v = \frac{v_0}{v_{dc}} \tag{11}$$

Averaged over a cycle

$$\begin{aligned} \frac{3}{2}v_0e^{j\alpha} &= dV_1V_{dc} + dV_2V_{dc}e^{j\frac{\pi}{3}} \\ dV_1 &= \left(\frac{\sqrt{3}v_0}{V_{dc}}\right)\sin(60-\alpha) \\ dV_2 &= \left(\frac{\sqrt{3}v_0}{V_{dc}}\right)\sin\alpha \end{aligned} \tag{12}$$

2.4 Indirect modulation of matrix converter

Indirect modulation of matrix converter can be explained using the hypothetical converter as shown in Figure 12. In this converter a CSI is connected to a VSI through what is called a virtual DC link. The AC or grid voltage side converter is modulated as CSI in order to rectify the balanced three phase input AC voltage to a virtual DC and to synthesize the average input current space vector aligned along the input voltage space vector to get input power factor correction. The output or the load side converter is modulated as a VSI in order to generate adjustable magnitude and frequency PWM AC at the load end.

Combined switching states of CSI and VSI results in the 18 active states of the matrix converter as specified before. For example when $V_2 [1 \ 1 \ 0]$ (S_{A1} , S_{B1} and S_{C2}) is applied on the VSI and I_3 (S_{b1} and S_{c2} are on) is applied on the CSI the resulting state of the matrix converter is [b b c]. Some of the combination of the switching states of CSI and VSI are shown in Table 1.

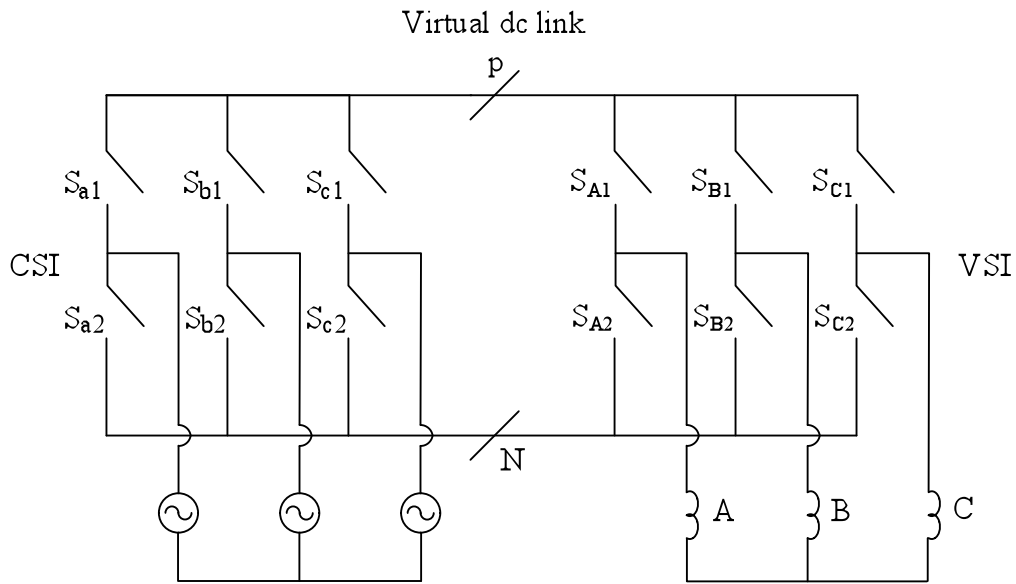


Figure 12. Indirect modulation of matrix converter

Say in a particular sampling cycle both I_{in} and V_{ref} are in the respective first sectors following switching states are applied over one sampling cycle. Where dI_1 , dI_2 , dV_1 and dV_2 are obtained from equations (6) and (12).

CSI	VSI	Duty Cycle
[a b]	[1 0 0]	$dI_1dV_1 = a b b$
[a b]	[1 1 0]	$dI_1dV_2 = a a b$
[a c]	[1 0 0]	$dI_2dV_1 = a c c$
[a c]	[1 1 0]	$dI_2dV_2 = a a c$

Table 1. Combined Switching States of CSI and VSI

2.5 Modulation scheme of the proposed topology

The modulation of the power electronic transformer presented in this thesis is based on indirect modulation of matrix converter. The topology of the proposed converter is shown in Figure 13. In this topology all of the switches need to be four quadrant, as they need to block voltages and flow currents in both direction. As discussed before these switches are obtained by the common emitter connection of two IGBTs.

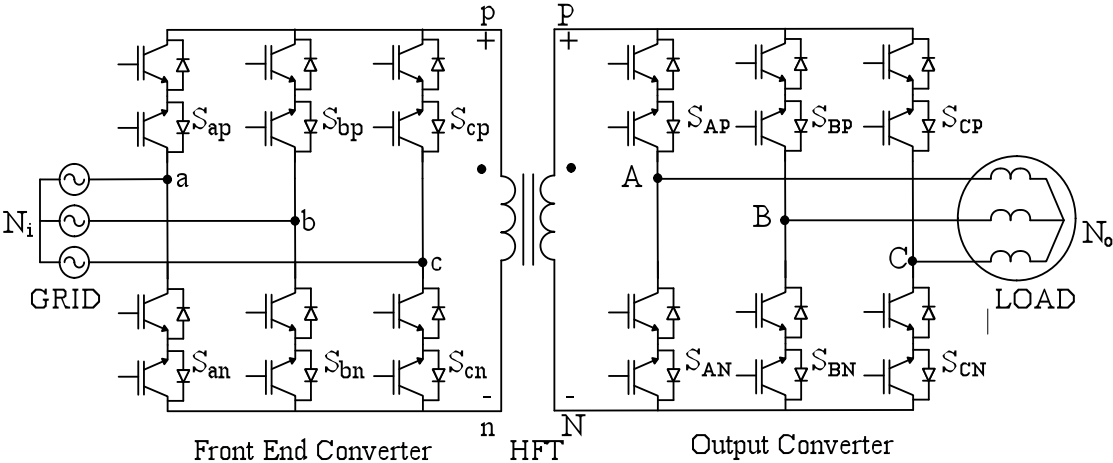


Figure 13. Circuit diagram of power electronic converter system

The input converter functions as a CSI and rectifies the input grid voltages to create a virtual DC link as in case of the hypothetical converter implementing indirect modulation as described in the previous section. The input converter also chops the virtual dc link with 50% duty cycle and generates high frequency AC. This high frequency AC voltage is applied to the primary of a single phase high frequency transformer (HFT). The output converter connected to the secondary of the HFT first rectifies the high frequency AC to get back the virtual DC link and then acts as a VSI to generate adjustable magnitude and frequency PWM AC at the load terminals.

Due to creation of the high frequency AC link (unlike the simple virtual DC link described in the previous section) 50% of the time CSI and output VSI are switched to

generate I_{ref} and V_{ref} respectively. Rest of the time both of these converters are modulated to synthesize $-I_{ref}$ and $-V_{ref}$,

Due to the presence of leakage inductances in the transformer windings each switching of the secondary or load side converter requires commutation of leakage energy leading to distortion in the output voltage, voltage loss, common mode voltage switching etc. The objective of the modulation presented in this work is to minimize the switching transitions of the secondary side converter in order to minimize the frequency of leakage commutation. Figure 15 shows how the voltage and current vectors are applied over a sampling cycle T_s . The output converter is switched only once over this period. The zero vectors are applied to the load with the help of input converter. SV_1 represents the switching signal corresponding to the vector V_1 of the output converter as shown in Figure 14.

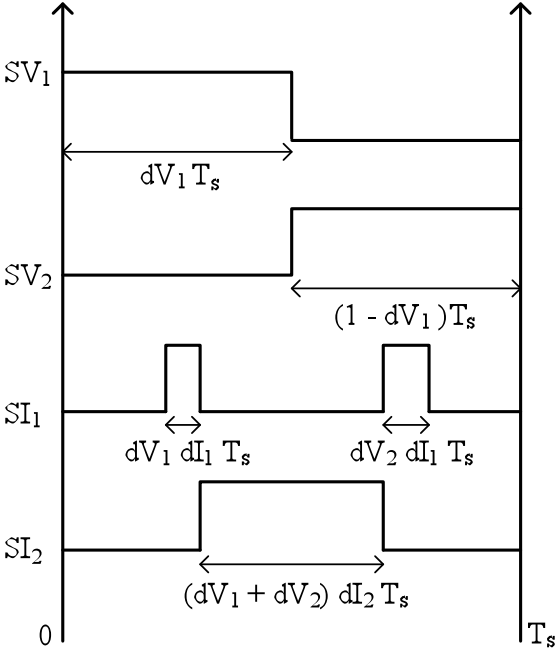


Figure 14. Generation of switching signals

Sequence of vectors applied over one complete cycle of flux balance is shown in Figure 15 (S being the flux balance signal).

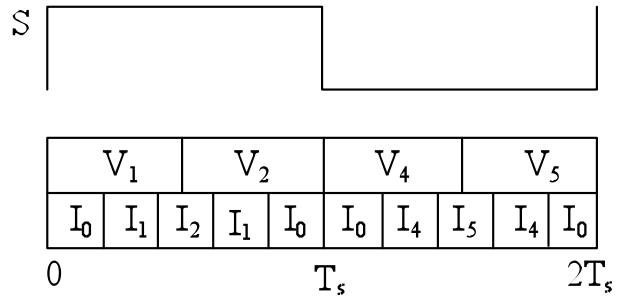


Figure 15. Application of Voltage and Current vectors over T_s

Chapter 3

Commutation

This chapter presents source-based commutation of leakage energy. The windings of the high frequency transformer contain leakage inductance. At each switching transition of the secondary or the load side converter the transformer winding current or the current through the leakage inductance has to change. Change in the current through an inductance requires application of a voltage. Usually a passive snubber or a clamp circuit is used for leakage commutation. In this process the leakage energy is lost. Use of additional circuits for commutation is not only energy inefficient, it adds to cost, reduces reliability and power density.

In this thesis the input source/grid voltage is used for the commutation of leakage energy. This results in soft switching of the output side converter but requires additional hard switching of the input side converter. So this process not only eliminates additional circuits but also results in the partial recovery of the leakage energy.

So leakage commutation occurs when the secondary side converter switches. There are basically two types of switching that happen in the secondary side converter, as explained in the previous chapter. First type of switching is when during a cycle of output voltage generation (T_s) the output converter switches from one active vector to the next active vector for example V_1 to V_2 as explained in the previous chapter. The other type of switching happens when the flux balance signal S changes its state i.e. V_2 changes to V_5 . Commutation due to both of these two types of transitions is explained in detail in the following subsection.

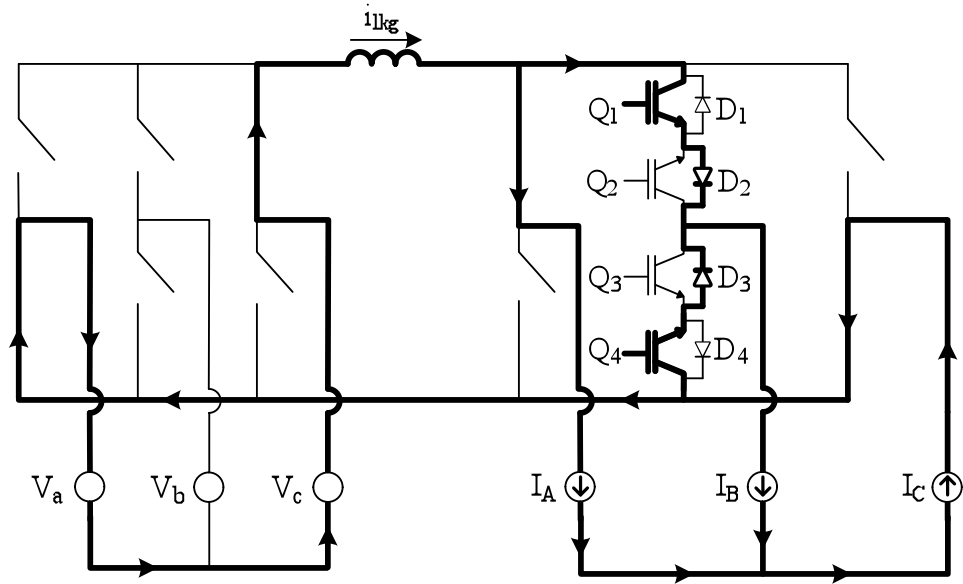


Figure 16. Commutation when output converter switches from one active vector to next

3.1 Commutation when output converter switches from one active vector to next

In this analysis we neglect the magnetizing inductance of the transformer and instead represent it as a series connection of primary and secondary leakage inductance (L_{lkg}). Due to the inductive nature of the output load any switching in the output converter leads to change in the current flowing through L_{lkg} . For example if switching from V_1 to V_2 it implies that leg B is switching. During a sampling cycle when the output converter switches from one active vector to the next, only one leg switches.

Input source voltage is used for commuting the current flowing through L_{lkg} . Depending upon the direction of flow of the load current of the particular phase which is connected to the leg which is undergoing switching and the type of switching which is taking place from bottom to top or top to bottom, there are four cases which are possible. Here I am describing one of the four cases in detail. Here we assume that the input current and the output voltages are DC sources (i.e. i_A as I_A and v_a as V_a) during commutation as shown in Figure 16. We can assume them to be DC as the commutation time is very small in comparison to the time periods of the input voltage and the output

current waveforms. In this example we are considering a transition from V_1 to V_2 as shown in Figure 16.

This implies leg B is undergoing a switching from bottom to top. Let us assume current I_B is positive. The leakage current $i_{lkg} = I_A$ initially. In the bidirectional switch pair Q_3 and Q_4 the non-conducting IGBT Q_3 is turned OFF. There after the IGBT Q_1 is turned ON and will start conducting in the bidirectional switch pair Q_1 and Q_2 . The current through L_{lkg} should increase as ultimately $i_{lkg} = I_A + I_B$ is to flow through the leakage inductance. As $I_B > 0$ we now need to apply maximum positive line to line voltage through the input converter which in this case is say V_{ca} . This causes diode D_2 to get forward biased and hence the current through L_{lkg} starts reducing. Here

$$V_{ca} = L_{lkg} \frac{di_{lkg}}{dt}$$

The current flowing through D_3 starts reducing till it reaches zero and the current flowing through D_2 starts increasing. When $i_{lkg} = I_A + I_B$ as the current through diodes D_2 and D_3 cannot reverse hence bringing the commutation to a natural end. The maximum estimated commutation time is $t_{com} = \frac{L_{lkg} I_o}{1.5V_{in}}$. After this Q_4 is turned

OFF and Q_2 is turned ON. The switching of $Q_{1,2,3,4}$ happens with Zero Current (ZCS).

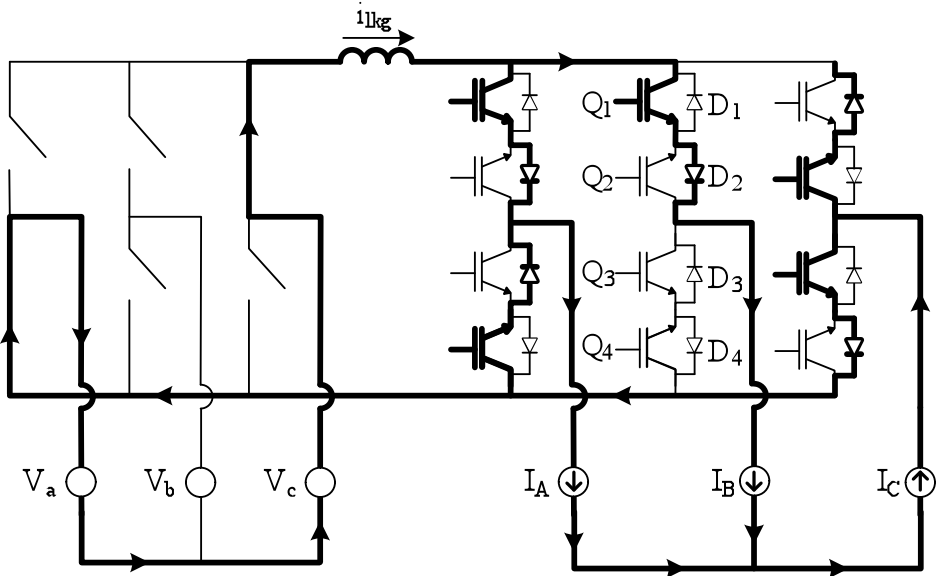


Figure 17. Commutation due to the transition of the flux balance signal

3.2 Commutation due to the transition of the flux balance signal

Output converter switches when the flux balance signal S changes its state as shown in Figure 17. In this transition as described in the modulation chapter two legs of the output converter switch when exactly the opposite vector is applied. For example output converter changes its state from V_2 to V_5 . This leads to a change in the current through the leakage inductance ($I_A + I_B$ to $I_B + I_C$). With the knowledge of the three output line currents and from the switching state of the output converter it is possible to estimate the change in i_{lkg} . So depending on the change in the current through the leakage inductance a positive or a negative (maximum line to line) voltage is applied using the input converter. The switching of the two legs of output converter is exactly similar to that described for a single leg in the previous subsection. Again the switching transition of the output converter happens in zero current (ZCS).

Chapter 4

Simulation Results

4.1 Parameters used in simulation

The topology in Figure 13, along with the proposed control has been simulated in MATLAB/Simulink. The parameters for the simulation like input voltage V_i , load impedance R_{Load} , L_{Load} , leakage inductance L_{lkg} , input frequency ω_i , output frequency ω_0 for modulation for CSI and VSI are as shown in Table 2.

V_i	$500 \sqrt{2} \text{ V}$	$f_s = 1/T_s$	5kHz
R_{load}	8Ω	ω_0	$2\pi 60 \text{ rad/s}$
L_{load}	12.7mH	ω_i	$2\pi 60 \text{ rad/s}$
L_{lkg}	100 μ H	m_I	1
L_m	10mH	m_V	0.4
N_2 / N_1	1		

Table 2. Parameters for simulation

4.2 Results of simulation

Figure 18 shows simulated output line to neutral voltage and line current of phase A. The peak of the output line current is slightly lower than its analytically predicted value (Analytical $I_A = 22.73\text{A}$, Simulated $I_A = 21.4\text{A}$). This is due to the loss of output voltage during commutation.

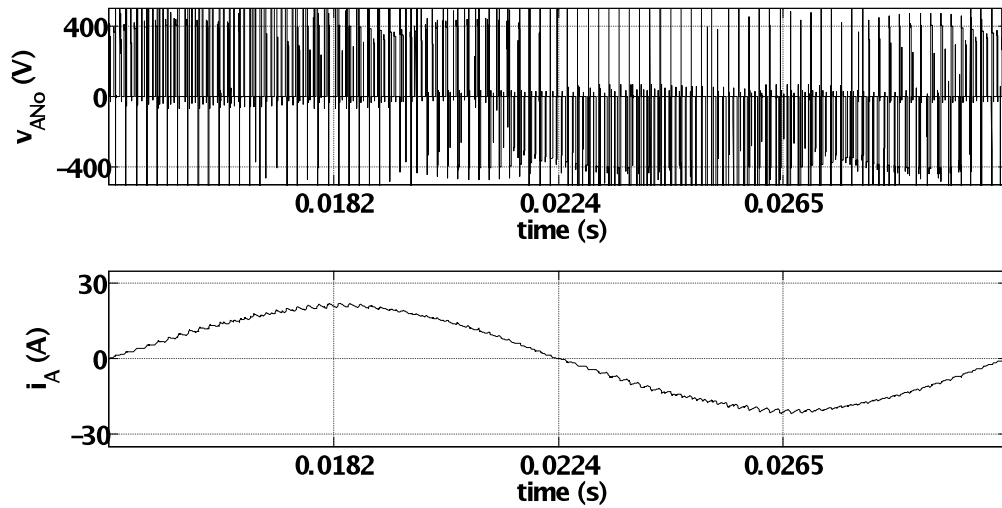


Figure 18. Simulation result: output line to neutral voltage & output line current

Figure 19 shows the filtered input current in phase along with the corresponding input line to neutral voltage hence verifying input power factor correction.

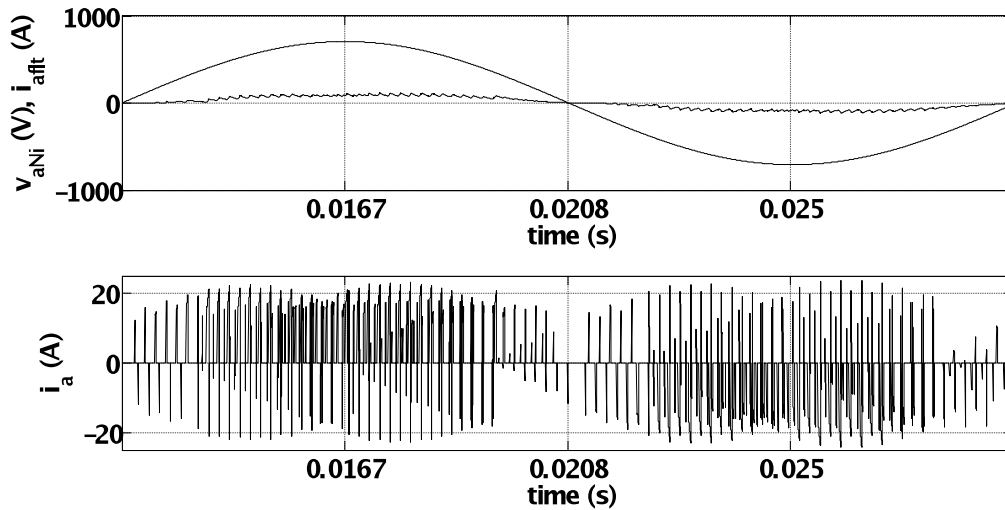


Figure 19. Simulation result: a) input line to neutral voltage with filtered input line current (20A/div) b) actual input line current

Figure 20 shows commutation of leakage inductance current when the output converter is making a transition from [011] to [001].

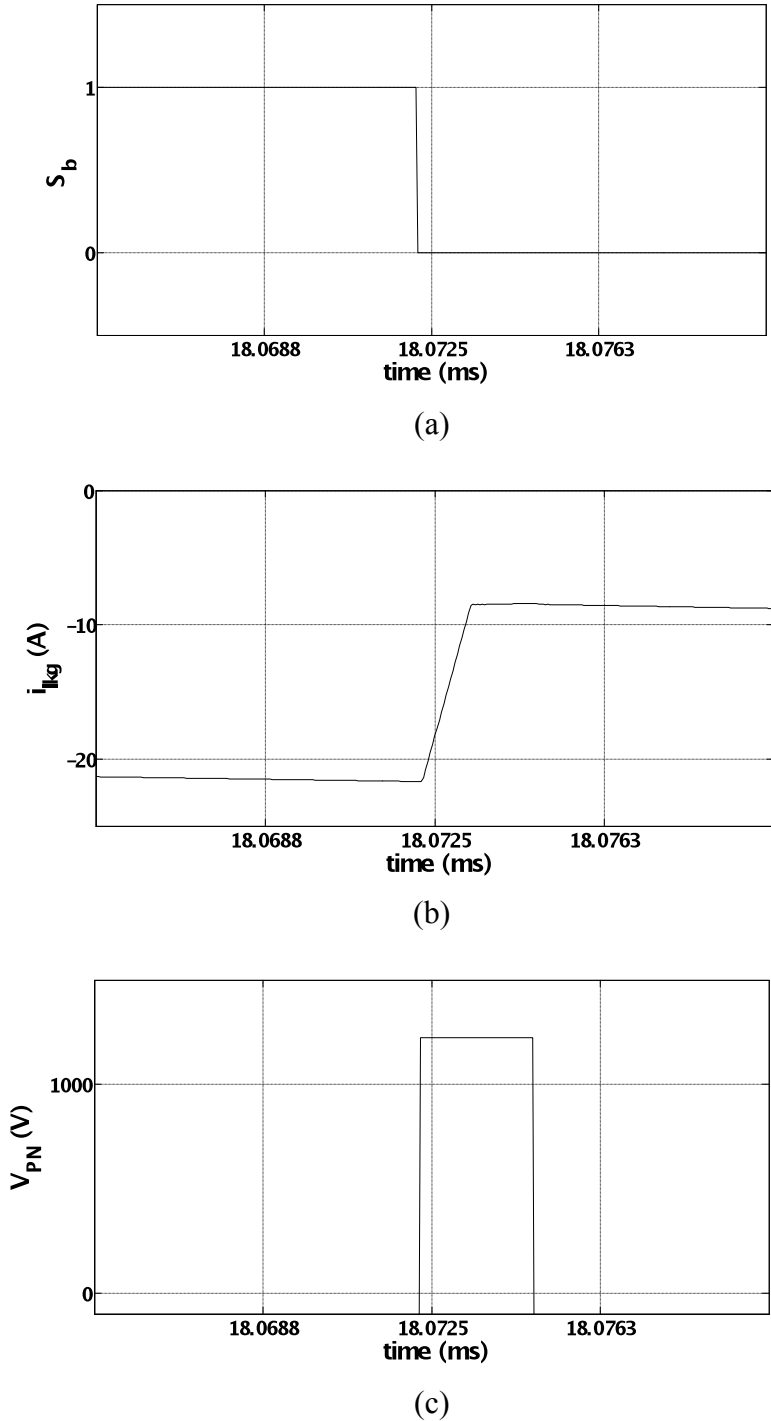


Figure 20. Simulation result: commutation of leakage inductance current

In Figure 20(a) leg B is switching from top to bottom. The leakage inductance current linearly changes from $I_B + I_C = -22\text{A}$ to $I_C = -8.5\text{A}$, as in Figure 20(b). The slope of the linear rise matches with the analytical predictions. This change in the current i_{lkB} requires a positive V_{PN} . In Figure 20(c) $V_{ac} = 1225\text{V}$ was the maximum line to line voltage at that instant of time.

The magnetizing current of the transformer over one cycle of S is shown in Figure 21. This verifies flux balance.

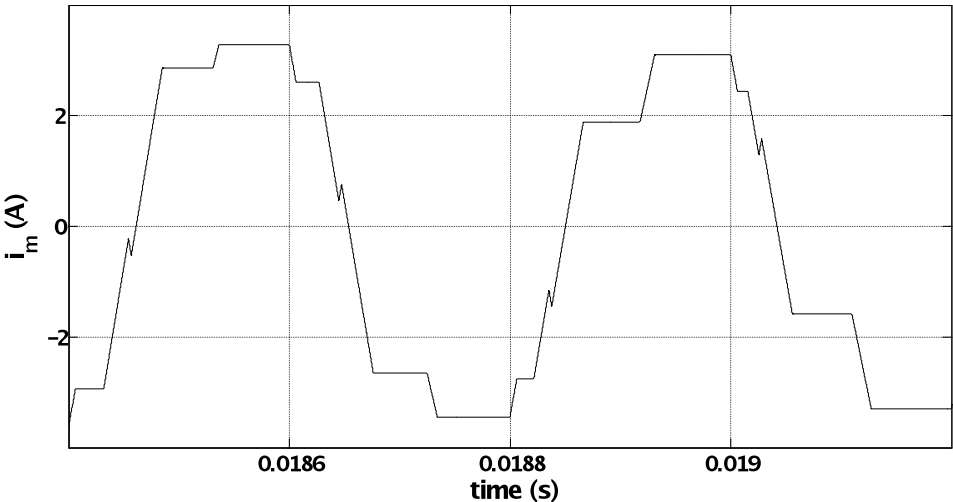


Figure 21. Simulation result: magnetizing current

Chapter 5

Experimental Results

5.1 Experimental set up

The input side converter has 6 bidirectional switches (two common emitter connected IGBTs). For implementing this, an integrated power module (IPM) from Microsemi (APTGT75DU120TG) is used. Gate resistance R_G is chosen to be 18 ohms to obtain the difference in ON and OFF time of IGBT to be equal to 600 ns. This time is the basis for choosing 4 step commutation of converter and the time for different states of the output converter during commutation.

To generate the PWM signals, an FPGA based control platform (Xilinx XC3S500E) has been used. Hall effect sensors followed by Sallen Key filters of bandwidth of 250 KHz are used for sensing the three output load currents, and the three input line voltages. It is sufficient to use a low bandwidth sensor as the sensed signal is at a low frequency (10 to 100 Hz). For the output currents it is important to note that only direction is required for leakage inductance commutation. The control platform consists of a 12 bit ADC (ADC7366).

The transformer has $N_1:N_2 = 1:1$ turns ratio and its design is done using the area product method. The average value of volt seconds applied to the primary of the transformer is $\frac{VT_s}{2}$. From this the following equation (13) is obtained.

$$A_c = \frac{V}{4N_1 B_{peak} f_s} \quad (13)$$

Here A_c is the core area, B_{peak} is the peak flux density and N_1 is the number of turns of the primary winding and N_2 is the number of turns of the secondary winding. The effective window area is given by equation (14)

$$A_w k_w = \frac{2N_1 I_1}{J} \quad (14)$$

Here A_w is the window area and, k_w is the window fill factor, I_1 is the current in the primary winding and J is the current density. By using the area product method it was determined that a FINEMET C core should be used for the transformer.

5.2 Experimental Results

This section presents the experimental results that verify the behavior predicted by analysis and simulation results shown in the previous chapters. The parameters for the experimental set up are given in Table 3.

L_{load}	R_{load}	L_{lkg}	L_m	$\frac{N_2}{N_1}$	V_i	$f_s = \frac{1}{T_s}$	ω_o	ω_i
23 mH	5 Ω	28 μ H	180 mH	1	45 $\sqrt{2}$ V	5 kHz	2 π 27.5 rad/s	2 π 60 rad/s

Table 3. Parameters in experimental set up

Figure 22 shows the input voltage and the filtered input current. The input current is in phase with the input voltage. This confirms the input power factor correction. Figure 23 shows the output load voltage and the output currents for a balanced three phase R-L load. The three phase load acts as a low pass filter and removes the response due to high frequency switching of the IGBTs. Figure 24 shows the output currents at output frequency of 11 Hz when a three phase induction motor loaded with a dc generator is run in V/f mode (=3). The input voltage is at a frequency of 60 Hz. Figure 25 shows the measured secondary or the leakage induction current along with the primary voltage over one cycle of S signal. Figure 26 shows these waveforms on an expanded scale.

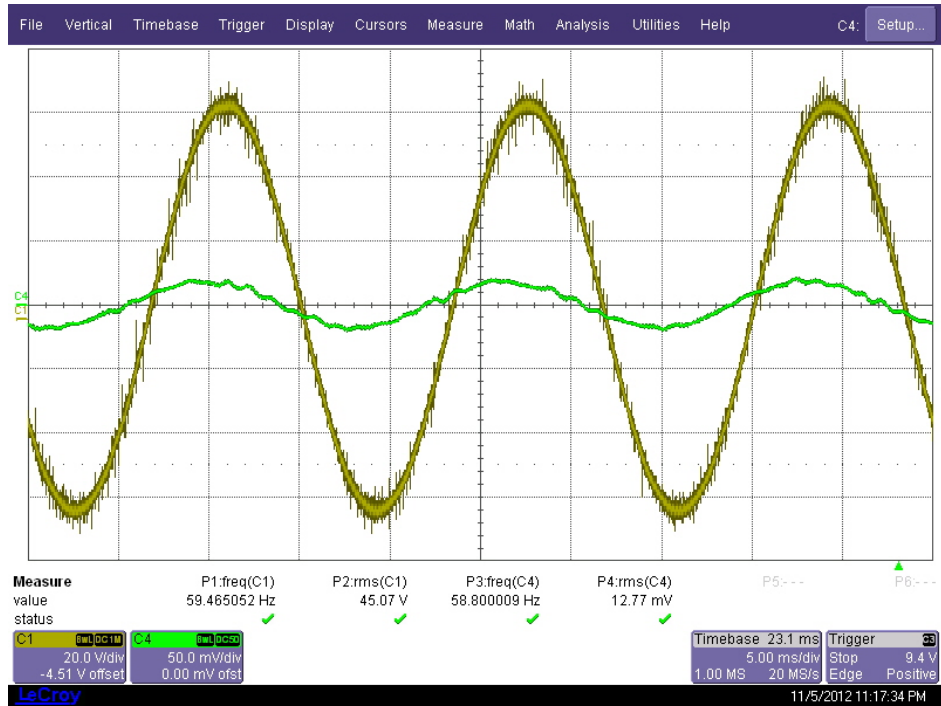


Figure 22. Input line voltage CH1 (20V/div), and input current CH4 (5A/div)

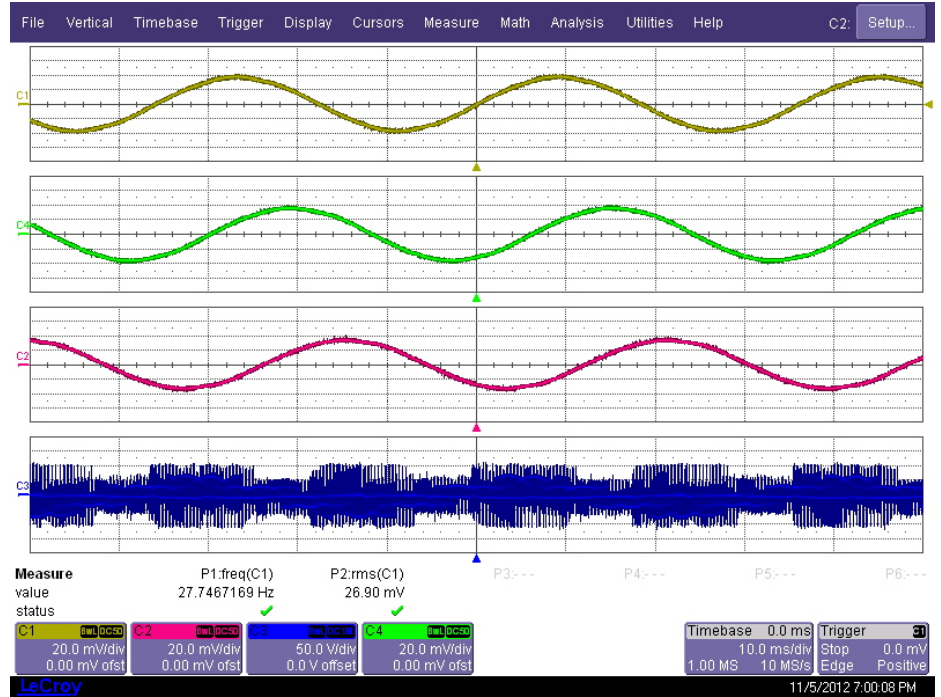


Figure 23. Output line to neutral voltage CH3 (50 V/div), line currents CH1, CH2 and CH4 (5A/div) and time (50 ms/div)

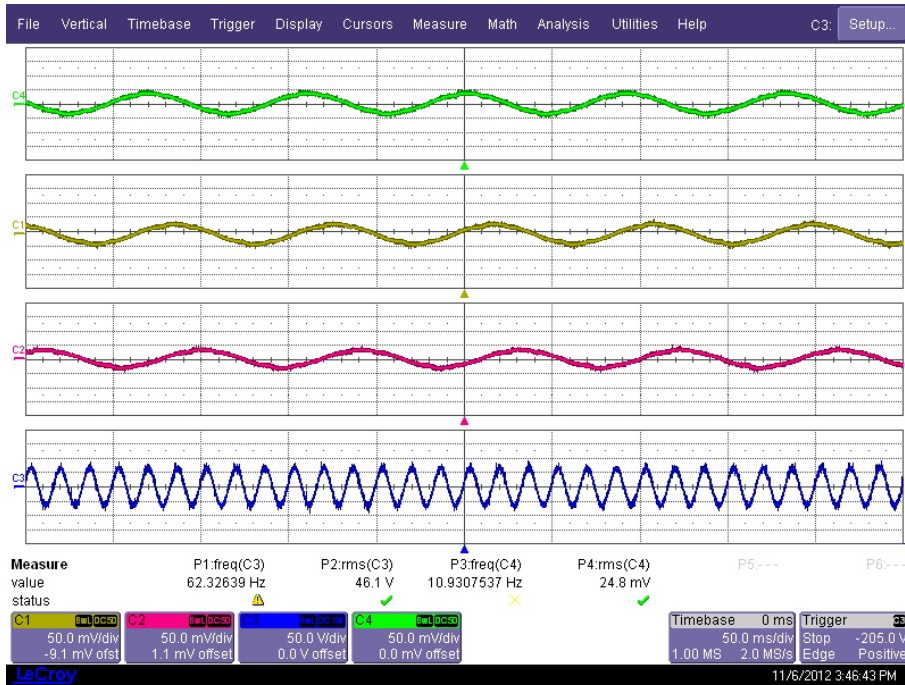


Figure 24. Input line to neutral voltage CH3 (50 V/div), and line currents CH1, CH2 and CH4 and time (50 ms/div)

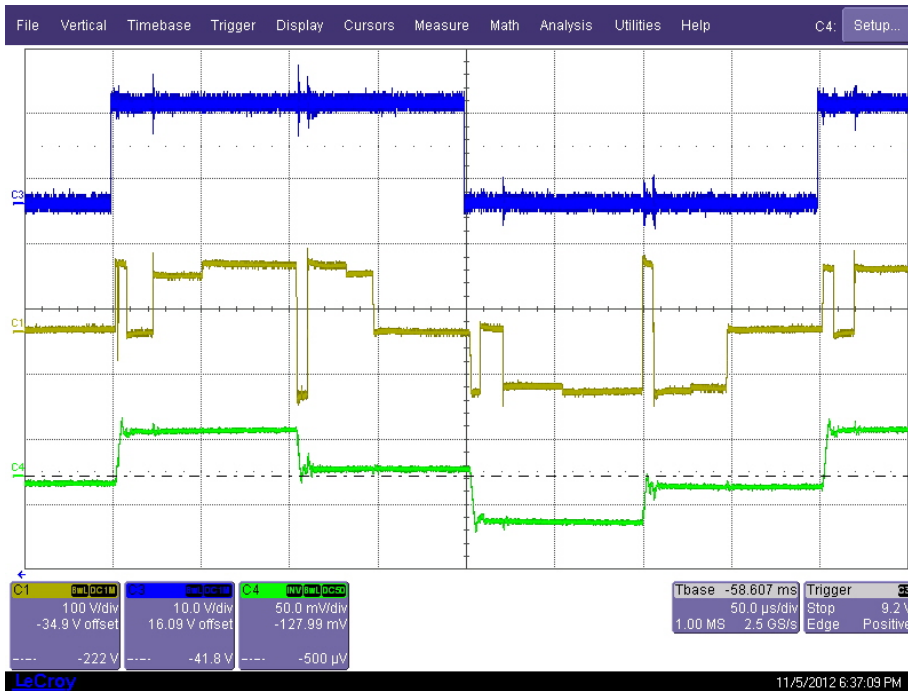


Figure 25. Control voltage (S Signal) CH3 (10V/div), primary voltage CH1 (100V/div), leakage inductance current CH4 (5A/div) and time (50 μS/div)

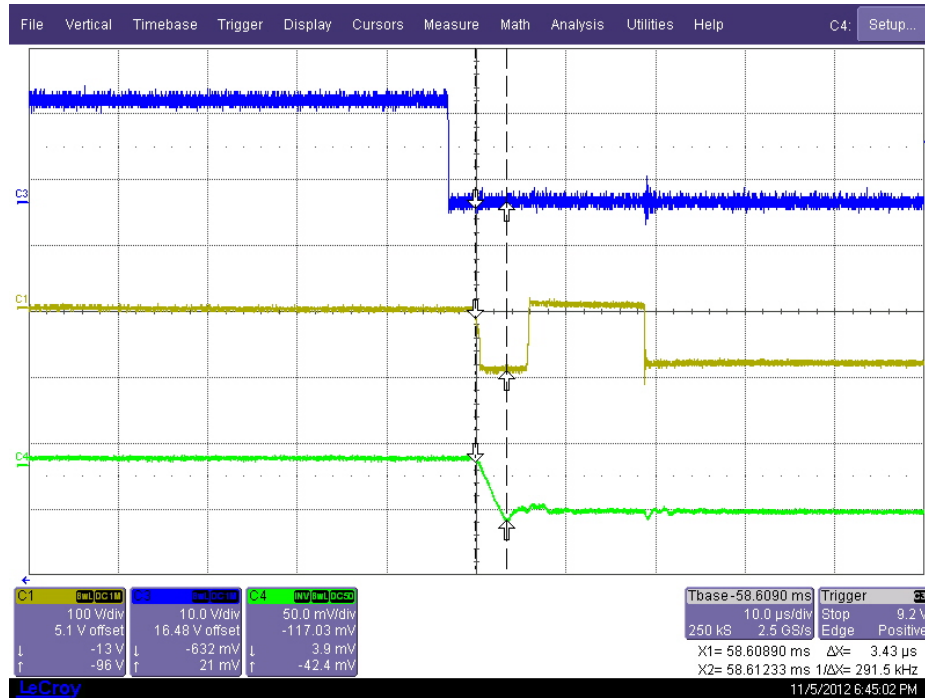


Figure 26. Expanded view of the waveform in Figure 25

5.3 Comparison of Analytic and Experimental Results

The measured experimental result gives value of commutation time close to analytical value. The transition of current using source based commutation is smooth and matches well with commutation time predicted by the equation:

$$t_{com} = \frac{L_{lkg} I_o}{1.5V_{in}}$$

The behavior of commutation as observed in experimental setup matches well with that in simulations. The voltage levels used in simulation are realistic corresponding to actual available voltages, but in experimental setup lower voltages are used for safety reasons. Hence a value by value match is not expected. But the experimental measurement validates the theory proposed in value as well as overall behavior.

Chapter 6

Conclusion

This thesis presents a novel switching strategy based on the control of the indirect matrix converter for a three phase AC-AC converter with a high frequency transformer. The topology based on the indirect modulation of matrix converter has the following advantages:

1. High power density.
2. Galvanic isolation.
3. Single stage power conversion.
4. Input power factor correction.
5. Less number of semiconductor switches (equal in primary as well as secondary side).
6. It uses minimum amount of copper.

In this thesis a novel modulation method along with a commutation technique has been proposed. This not only preserves all of the previously mentioned advantages but also results in the following:

- a) Lossless commutation in leakage energy.
- b) Soft switching of output converter (ZCS).
- c) Minimization of the frequency of leakage inductance commutation leading to less output voltage loss and increased frequency of operation.

The analysis of this converter has been done in detail. The topology along with the proposed control technique has been simulated and verified experimentally. The simulation and experimental results clearly verify the advantages stated above.

References

- [1] W. M. Murray, “Power conversion circuit having a high frequency link,” *US Patent Application US3.517.300*, April 1968.
- [2] E. Ronan, S. Sudhoff, S. Glover, and D. Galloway, “A power electronic- based distribution transformer,” *Power Delivery, IEEE Transactions on*, vol. 17, no. 2, pp. 537–543, April 2002.
- [3] C. G. C. Branco, R. Torrico-Bascope, C. M. T. Cruz, and F. de A Lima, “Proposal of three-phase high-frequency transformer isolation ups topologies for distributed generation applications,” *Industrial Electronics, IEEE Transactions on*, vol. 60, no. 4, pp. 1520–1531, April. 2013.
- [4] A. Garces and M. Molinas, “A study of efficiency in a reduced matrix converter for offshore wind farms,” *Industrial Electronics, IEEE Transactions on*, vol. 59, no. 1, pp. 184–193, 2012.
- [5] X. She, A. Huang, F. Wang, and R. Burgos, “Wind energy system with integrated functions of active power transfer, reactive power compensation, and voltage conversion,” *Industrial Electronics, IEEE Transactions on*, vol. PP, no. 99, p. 1, 2012.
- [6] P. Drabek, Z. Peroutka, M. Pittermann, and M. Cedi, “New configuration of traction converter with medium-frequency transformer using matrix converters,” *Industrial Electronics, IEEE Transactions on*, vol. 58, no. 11, pp. 5041–5048, 2011.
- [7] M. Carpita, M. Marchesoni, M. Pellerin, and D. Moser, “Multilevel converter for traction applications: Small-scale prototype tests results,” *Industrial Electronics, IEEE Transactions on*, vol. 55, no. 5, pp. 2203–2212, 2008.
- [8] M. Glinka and R. Marquardt, “A new ac/ac multilevel converter family,” *Industrial Electronics, IEEE Transactions on*, vol. 52, no. 3, pp. 662–669, 2005.

- [9] H. Krishnamoorthy, P. Enjeti, I. Pitel, and J. Hawke, “New medium-voltage adjustable speed drive (asd) topologies with medium-frequency transformer isolation,” in *Power Electronics and Motion Control Conference (IPEMC), 2012 7th International*, vol. 2, June 2012, pp. 814–819.
- [10] S. Falcones, X. Mao, and R. Ayyanar, “Topology comparison for solid state transformer implementation,” in *Power and Energy Society General Meeting, 2010 IEEE*, 2010, pp. 1–8.
- [11] X. She, R. Burgos, G. Wang, F. Wang, and A. Huang, “Review of solid state transformer in the distribution system: From components to field application,” in *Energy Conversion Congress and Exposition (ECCE), 2012 IEEE*, 2012, pp. 4077–4084.
- [12] M. Banaei and E. Salary, “Power quality improvement based on novel power electronic transformer,” in *Power Electronics, Drive Systems and Technologies Conference (PEDSTC), 2011 2nd*, 2011, pp. 286–291.
- [13] M. Sabahi, S. Hosseini, M. Sharifian, A. Goharrizi, and G. Gharehpetian, “Zero-voltage switching bi-directional power electronic transformer,” *Power Electronics, IET*, vol. 3, no. 5, pp. 818–828, 2010.
- [14] G. Wang, S. Baek, J. Elliott, A. Kadavelugu, F. Wang, X. She, S. Dutta, Y. Liu, T. Zhao, W. Yao, R. Gould, S. Bhattacharya, and A. Huang, “Design and hardware implementation of gen-1 silicon based solid state transformer,” in *Applied Power Electronics Conference and Exposition (APEC), 2011 Twenty-Sixth Annual IEEE*, 2011, pp. 1344–1349.
- [15] S. Bifaretti, P. Zanchetta, A. Watson, L. Tarisciotti, and J. Clare, “Advanced power electronic conversion and control system for universal and flexible power management,” *Smart Grid, IEEE Transactions on*, vol. 2, no. 2, pp. 231–243, 2011.
- [16] J.-S. Lai, A. Maitra, A. Mansoor, and F. Goodman, “Multilevel intelligent universal transformer for medium voltage applications,” in *Industry Applications Conference, 2005. Fortieth IAS Annual Meeting. Conference Record of the 2005*,

- vol. 3, 2005, pp. 1893–1899 Vol. 3.
- [17] H. Fan and H. Li, “High-frequency transformer isolated bidirectional dc dc converter modules with high efficiency over wide load range for 20 kva solid-state transformer,” *Power Electronics, IEEE Transactions on*, vol. 26, no. 12, pp. 3599–3608, 2011.
- [18] M. Kang, P. Enjeti, and I. Pitel, “Analysis and design of electronic transformers for electric power distribution system,” in *Industry Applications Conference, 1997. Thirty-Second IAS Annual Meeting, IAS '97., Conference Record of the 1997 IEEE*, vol. 2, Oct 1997, pp. 1689–1694 vol.2.
- [19] H. Krishnaswami and V. Ramanarayanan, “Control of high-frequency ac link electronic transformer,” *Electric Power Applications, IEE Proceedings*, vol. 152, no. 3, pp. 509–516, 6 May 2005.
- [20] D. Chen and J. Liu, “The uni-polarity phase-shifted controlled voltage mode ac-ac converters with high frequency ac link,” *Power Electronics, IEEE Transactions on*, vol. 21, no. 4, pp. 899–905, July 2006.
- [21] K. Harada, F. Anan, K. Yamasaki, M. Jinno, Y. Kawata, and T. Nakashima, “Intelligent transformer,” in *Power Electronics Specialists Conference, 1996. PESC '96 Record, 27th Annual IEEE*, vol. 2, June 1996, pp. 1337–1341 vol.2.
- [22] R. A. Xiaolin Mao and S. Falcones, “A modular, interleaved ac-ac flyback topology for solid state transformer,” in *FREEDM Annual Conference 2009, North Carolina State University, Raleigh, NC*, May 2009, pp. 221–224.
- [23] M. Manjrekar, R. Kieferndorf, and G. Venkataramanan, “Power electronic transformers for utility applications,” in *Industry Applications Conference, 2000. Conference Record of the 2000 IEEE*, vol. 4, Oct 2000, pp. 2496–2502 vol.4.
- [24] H. Qin and J. Kimball, “Ac-ac dual active bridge converter for solid state transformer,” in *Energy Conversion Congress and Exposition, 2009. ECCE 2009. IEEE*, 2009, pp. 3039–3044.
- [25] H. Keyhani, H. Toliyat, M. Todorovic, R. Lai, and R. Datta, “Isolated soft-switching hf ac-link 3-phase ac-ac converter using a single-phase hf transformer,”

- in *IECON 2012 - 38th Annual Conference on IEEE Industrial Electronics Society*, 2012, pp. 512–517.
- [26] P. Wheeler, J. Rodriguez, J. Clare, L. Empringham, and A. Weinstein, “Matrix converters: a technology review,” *Industrial Electronics, IEEE Transactions on*, vol. 49, no. 2, pp. 276–288, April 2002.
- [27] K. Basu, R. K. Gupta, S. Nath, G. F. Castelino, K. K. Mohapatra, and N. Mohan, “Research in matrix-converter based three-phase power- electronic transformers,” in *Power Electronics Conference (IPEC), 2010 International*, jun. 2010, pp. 2799–2803.
- [28] R. K. Gupta, K. K. Mohapatra, and N. Mohan, “A novel three-phase, switched multi-winding power electronic transformer,” in *Proc. IEEE Energy Conversion Congress and Exposition (ECCE) 2009*, San Jose, CA, Sep. 2009, pp. 2696 – 2703.
- [29] G. Castelino, K. Basu, R. Gupta, and N. Mohan, “Power electronic transformer with reduced number of switches: Analysis of input clamp circuit and a modulation strategy to eliminate input snubber requirement,” in *IECON-USA*, 2010.
- [30] K. Basu and N. Mohan, “A power electronic transformer for three phase pwm ac/ac drive with loss less commutation and common-mode voltage suppression,” in *IECON 2010 - 36th Annual Conference on IEEE Industrial Electronics Society*, nov. 2010, pp. 315–320.
- [31] L. Huber and D. Borojevic, “Space vector modulated three-phase to three-phase matrix converter with input power factor correction,” *Industry Applications, IEEE Transactions on*, vol. 31, no. 6, pp. 1234–1246, November / December 1995.
- [32] H. Cha and P. Enjeti, “A three-phase ac/ac high-frequency link matrix converter for vsfc applications,” in *Power Electronics Specialist Conference, 2003. PESC '03. 2003 IEEE 34th Annual*, vol. 4, June 2003, pp. 1971–1976 vol.4.
- [33] K. Basu, A. Umarikar, K. Mohapatra, and N. Mohan, “High-frequency transformer-link three-level inverter drive with common-mode voltage

- elimination,” in *Power Electronics Specialists Conference, 2008. PESC 2008. IEEE*, June 2008, pp. 4413–4418.
- [34] M. Matsui, M. Nagai, M. Mochizuki, and A. Nabae, “High-frequency link dc/ac converter with suppressed voltage clamp circuits-naturally commutated phase angle control with self turn-off devices,” *Industry Applications, IEEE Transactions on*, vol. 32, no. 2, pp. 293–300, Mar/Apr 1996.
- [35] S. Mazumder and A. K. Rathore, “Primary-side-converter-assisted soft- switching scheme for an ac/ac converter in a cycloconverter-type high- frequency-link inverter,” *Industrial Electronics, IEEE Transactions on*, vol. 58, no. 9, pp. 4161–4166, Sept. 2011.
- [36] G. Castelino, K. Basu, and N. Mohan, “Power electronic transformer with reduced number of switches: Analysis of clamp circuit for leakage energy commutation,” in *Power Electronics, Drives and Energy Systems (PEDES) 2010 Power India, 2010 Joint International Conference on*, December 2010, pp. 1 –8.
- [37] A. Shahani, K. Basu, and N. Mohan, “A power electronic transformer based on indirect matrix converter for pwm ac drive with lossless commutation of leakage energy,” in *Power Electronics, Machines and Drives (PEMD 2012), 6th IET International Conference on*, March 2012, pp. 1–6.